A Study on an In-Process Laser Localized Pre-Deposition Heating Approach to Reducing FDM Part Anisotropy

by

Abinesh Kurapatti Ravi

A Thesis Presented in Partial Fulfillment
of the Requirements for the Degree
Master of Science

Approved July 2016 by the
Graduate Supervisory Committee:

Keng Hsu, Chair
Owen Hildreth
Liping Wang

ARIZONA STATE UNIVERSITY

August 2016

ABSTRACT

Material extrusion based rapid prototyping systems have been used to produce prototypes for several years. They have been quite important in the additive manufacturing field, and have gained popularity in research, development and manufacturing in a wide field of applications. There has been a lot of interest in using these technologies to produce end use parts, and Fused Deposition Modeling (FDM) has gained traction in leading the transition of rapid prototyping technologies to rapid manufacturing. But parts built with the FDM process exhibit property anisotropy. Many studies have been conducted into process optimization, material properties and even post processing of parts, but were unable to solve the strength anisotropy issue. To address this, an optical heating system has been proposed to achieve localized heating of the pre-deposition surface prior to material deposition over the heated region. This occurs in situ within the build process, and aims to increase the interface temperature to above glass transition (T_g), to trigger an increase in polymer chain diffusion, and in extension, increase the strength of the part. An increase in flexural strength by 95% at the layer interface has been observed when the optical heating method was implemented, thereby improving property isotropy of the FDM part. This approach can be designed to perform real time control of inter-filament and interlayer temperatures across the build volume of a part, and can be tuned to achieve required mechanical properties.

ACKNOWLEDGMENTS

I would like to sincerely thank my advisor, Dr. Keng Hao Hsu, for providing me an opportunity to work with him. His support mechanism, guidance at every step, and the will to drive towards gaining more knowledge has helped me through the course of this thesis.

I would also like to thank Dr. Owen Hildreth and Dr. Liping Wang for agreeing to be on my thesis committee, and guiding me through the project and imparting me with their knowledge.

I would like to thank Anagh Deshpande and Sihan Zhang for taking the time off their own research to help me with obtaining certain results of my work. I would also like to thank Raymond Churchwell, Mazin Mohammad, Scott Kusel, Julie Cease, Ram Telikicherla and Lucas Casanova for guiding me through the course of the thesis.

I would also like to thank Mrs. Diana Convey of the Center for Solid State sciences at ASU and Dr. Emmanuel Soignard helping me with obtaining results from equipment at the CSS laboratories.

Finally I would like to thank all my friends and family for all their help and support.

TABLE OF CONTENTS

Page

CHAPTER Page

LIST OF TABLES

LIST OF FIGURES

Figure Page

1. INTRODUCTION

Rapid prototyping (RP) emerged as a technological alternative to conventional machining processes, to produce functional prototypes from CAD models. 3D systems was the first to develop and commercialize the Stereo-lithography (SLA) technic which presented a base for future RP processes. Solid Freeform fabrication, also described as Layered Manufacturing, was a major technology in the RP world. With these technologies gaining traction, additive manufacturing has gained a lot of popularity and has supplemented conventional subtractive manufacturing in certain scenarios.

Rapid Prototyping systems follow a set procedure when employed to build a product.

1) CAD model - using softwares like AutoCAD or SolidWorks, the part is designed digitally
2) CAD model Slicing - The part is sliced into multiple layers by soft wares like Slic3r or Cura, and G-codes tool paths are obtained as the output.
3) Part Build – The layer by layer information is sent to the printing machine through software interfaces such as PrintRun, and the entire part is built.

Shown in figure 1 is a representation of the process:

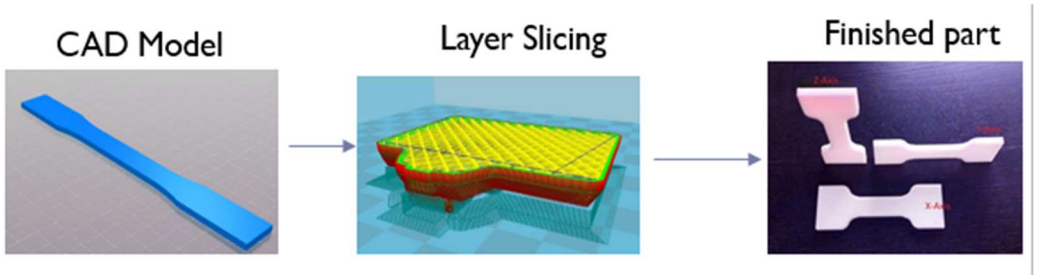

Figure 1 The Rapid Prototyping Process

The next section gives a brief overview of one of the major RP processes prevalent in the industry, the Fused Deposition Modeling (FDM).

1.1 Fused Deposition Modeling

Fused Deposition Modeling is a very robust and prominent Rapid Prototyping technology, which involves extruding a filament of Thermoplastic polymer like ABS, PLA, PETG etc, through a nozzle, heated to above the Glass transition temperature. The extrudate is deposited onto a heated bed or a pre-deposition surface, in the X-Y direction, layer by layer, to build the whole part. The parts are sliced based on conditions pre-determined by the software, based on the user's parametric inputs such as nozzle speed, layer thickness, raster type and number of perimeters, and the type of FDM machine being used. For instance, the user might want a precise rendering of the product, which would require inputs like slower nozzle speed or smaller layer thickness for a better part finish. The slices are sent to the machine in terms of layer-by-layer tool path information. FDM was developed by Stratasys Corporation© and produced machines such as the Stratasys 400MC to implement the process in a controlled and effective manner. The original patent for this technology expired recently, and a large number of product developers came out with their own versions of FDM machines, which decentralized the adoption of FDM across markets.

The FDM process follows the above-mentioned procedures for building parts. Once the G-codes containing tool path information are pushed to the machine, the material, which is in filament form, is pushed into the heated nozzle by rollers. The filament is softened and is extruded onto the pre-deposition surface, and the structure is

built layer by layer. Figure 2 is an illustration of the FDM process.

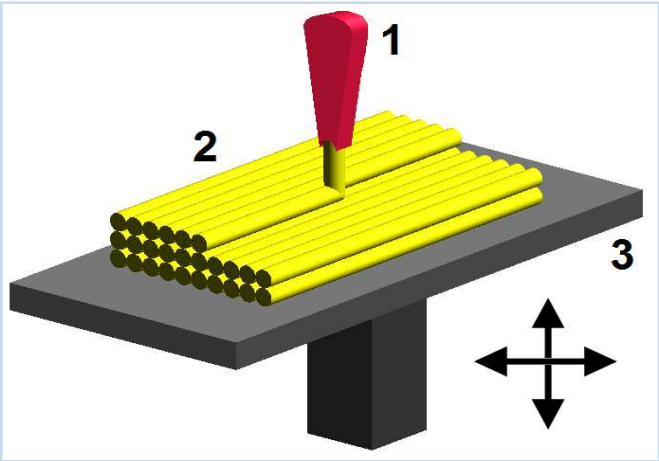

Figure 2 Layer By Layer Filament Deposition of the FDM Process [39]

The layer-by-layer process accommodated printing of thermoplastics in various configurations, and complex orientations. This allows great freedom in part design and printing. FDM has its strengths in durability, material flexibility and simplicity, but it has a tradeoff in terms of anisotropy in strength in the build direction. Inter-layer strength is much lower than along the filament strength, which is essentially the material property, and the material itself carries the load. The interlayer bond strength is much lower than the material strength, and this presents the anisotropy issue. Figure 3 represents the anisotropy as a schematic, while Figure 4 gives a numerical idea about anisotropy.

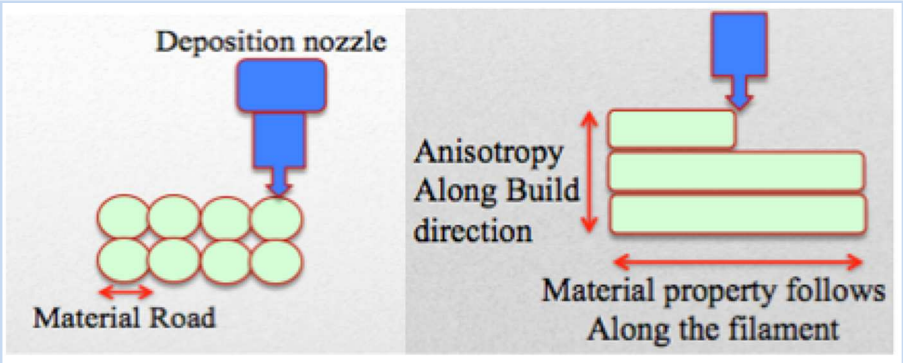

Figure 3 FDM Part Anisotropy

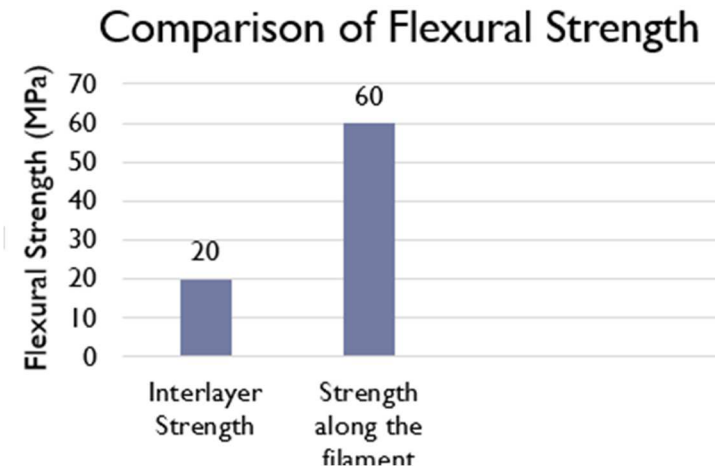

Figure 4 Flexural Strength Comparison within a FDM Build Part

Anisotropy effects can be reduced up to a point by methods like changing build orientation and path of build by the nozzle to map out a geometry that can take the load applied along the filament. But unexpected failure may occur if loading conditions change, and this is detrimental to the industry, which makes functional parts for the market. Therein lies the scope for this thesis, to solve a major problem for the industry!

1.2 Goal of the Thesis

The goal of the research presented here is to reduce FDM part anisotropy by localized heating of the pre-deposition surface, prior to polymer filament deposition. Localized heating will increase the interface temperature to above glass transition, where polymer chain diffusion and bonding would take place. This external parameter would not directly affect intrinsic FDM parameters. Implementation of this process may face a few problems, which are predictable. The optical heating approach may cause material decomposition and evaporation, which is detrimental to the part strength and reduces its dimensional accuracy. Also, the beam spot has to be maintained in front of the nozzle during the build process to achieve true pre-deposition heating. With these ideas and design constrains in mind, the laser pre-deposition heating system was implemented on a desktop 3D printer.

The rest of the thesis details the procedures in obtaining pre-deposition surface and interface temperature profiles, flexural test results on the interface, surface morphology using SEM imaging, laser ablation profile measurements and road geometry mapping after process implementation. A follow up discussion on the results obtained will present an overall sense of the process capability, and recommendations will be made for pursuing additional work in this area.

2. LITERATURE REVIEW

Due to the popularity of the FDM process and its potential in additive manufacturing, usage and optimization technics have been and are constantly being developed to improve the overall quality and usability of the part being printed. Agarwal et al. looked into decreasing internal and surface flaws of ceramic or metal parts, and applied these strategies into the FDM deposition process [1]. Langrana et al. monitored the printing of FDM parts in situ by using a simulation system and video microscopy. Process parameters were tested and varied to obtain higher quality parts [2]. Also, Han *et al.* aimed at developing algorithms to obtain better layer finish and quality by planning the tool path. Anitha *et al.* employed statistical ANOVA to study the surface finish quality and looked at improving the layer finish of the surface by influencing the processing parameters [3].

A different approach has also been investigated in terms of materials and applications for the process of FDM. Darsall et al. Looked at the biomedical applications by employing scaffold structures printed using FDM [4,5]. Bellini et al. Observed and reported on work by a research group, along with Wu et al., in Rutgers University. They looked towards improving FDM mechanical properties by developing a new extrusion system to extrude ceramics [6,7]. Shofner et al. proposed developing ABS material reinforced with vapor grown Nano-fiber to create a composite with increased tensile strength. A 68% increase in stiffness was observed [8].

Thirdly, work in the field has been looking at optimization of FDM part strength by modeling and characterization technics. Bellini along with Guceri looking into finding material constants by orthotropic material modeling, and performing tensile tests of FDM parts [9]. Thomas *et al.* and Rodriguez *et al*. researched into optimization of mechanical part properties to enhance their performance, by coming up with design tools. It involved microstructure [10] as well as a look at bond strength of FDM printed ABS parts [11] a look at an optimization algorithm to boost part performance [12]. Yan *et al.* analyzed bond strength of wax parts built with FDM, and developed a term called bond potential, which measures the status of interface bonds [13].

Also, a lot of work has been done in investigating the effects of intrinsic FDM parameters like raster angle, extruder temperature, road widths, etc., on the part flexural strength and residual stresses at the interface [14-32]. A conclusion that can be drawn from this is that one cannot obtain an optimal parametric set that can result in a strong part. A change in one of the intrinsic parameters would cause a negative change in another.

The literature review presented before shows a gap in improving FDM part strength in the build direction, except Rodriguez *et al.* and Yan *et al*., who address the issue of interlayer bonding directly. They explore using process parameters in determining bond strength or toughness, thereby optimizing inter-filament and inter-layer bond strength. In some studies, process parameters have been used to investigate bond formation taking plan when a hot polymer filament comes into contact with the

existing cold polymer filament. It has been observed that the critical parameters that determine bond strength are the nozzle temperature; build enclosure/environment temperature and the heat transfer occurring at the bond site [33, 34]. Build environment temperature has a greater effect on interlayer bond strength. It is understandable to think that increasing the build environment temperature is a good way to increase bond strength, but with it comes the associated problem of part dimensional inaccuracy and part finish. There was a study conducted by a team at Montana state university that developed a pre-deposition heating system to heat the pre-deposition surface with hot air during the part printing process [35]. Using hot air did not produce parts with higher strength, mainly due to non-localization of heat application, leading to uneven heating of the pre-deposition surface causing defects. But they did understand the approach, which resonated with earlier studies, that interface temperature needs to be high enough, and it should be maintained for some amount of time for the surfaces to undergo the three stages, which are wetting, diffusion and randomization, which was discussed in the reptation model proposed by De Gennes [36] and adopted by Wool *et al.* [37].

Based on the above literature about temperature and time being major factors in the strength of an interface, lets look a little closer at the FDM bonding process. Molecular bonding is achieved through interpenetration of molecular chains across the interface. Disappearance of this interface will be brought about ideally by larger interpenetration of molecular chains, thereby increasing the bond strength. This method of thermally induced mass diffusion occurs above glass transition temperature [Tg].

Yan *et al.* has described the process of molecular diffusion using Arrhenius equation:

$$\mathrm{dm} = -\mathrm{D}^{\circ}\, \mathrm{e}\hat{}\left(-\frac{\mathrm{Q}}{\mathrm{RT}}\left(\frac{\mathrm{dc}}{\mathrm{dx}}\right)\right) \mathrm{dt}$$

Where:

D_0 - Diffusion coefficient

Q - Activation energy

R – Gas constant

T - Interface temperature

c – Diffusion material concentration

x - Distance of diffusion

Diffusion coefficient is material dependent, and the concentration gradient at the interface is very difficult to map. Yan *et al.* introduced a term, i.e. bonding potential (ψ), to map the bonding process more effectively [38]:

$$\psi = \int \xi(\mathrm{T}) \,.\, e^{-\frac{k}{t}}\, dt$$

and,

$$\xi(\mathrm{T}) = 1 \; for \; T \geq Tc$$

$$\xi(\mathrm{T}) = 0 \; for \; T \leq Tc$$

Where,

T = Interface temperature

k = Bonding potential coefficient

T_c = Critical bonding temperature

An increase in bonding potential (ψ) shows a greater molecular bonding at the interface. Yan *et al.* performed experiments with processing conditions like Interface Temperature and performed load tests to compare the part strength to the bonding potential. A finite element model was developed to predict interlayer toughness by using interface temperature is a time dependent capacity.

Results of the studies presented here show that interface temperature has a major role in determining the bond strength, along with the nozzle and envelope temperatures. This thesis will look into influencing the interface temperature as a parameter to obtain higher part strength.

3. EXPERIMENTAL SETUP AND METHODOLOGY

Implementation of the optical heating system required experimentation to quantify the effects of increasing interlayer temperature. This chapter discusses the experimental designs, the procedures followed during experimentation and the conditions based on which the process variables were measured.

3.1 Process and Equipment Adaptation

3.1.1 Test Part Design

The goal of this thesis was to improve interlayer bonding by using optical pre-deposition heating of the pre-deposition surface. The test part was designed to undergo loading tests to determine the degree to which this strength has increased. The test part design is shown in Figure 5.

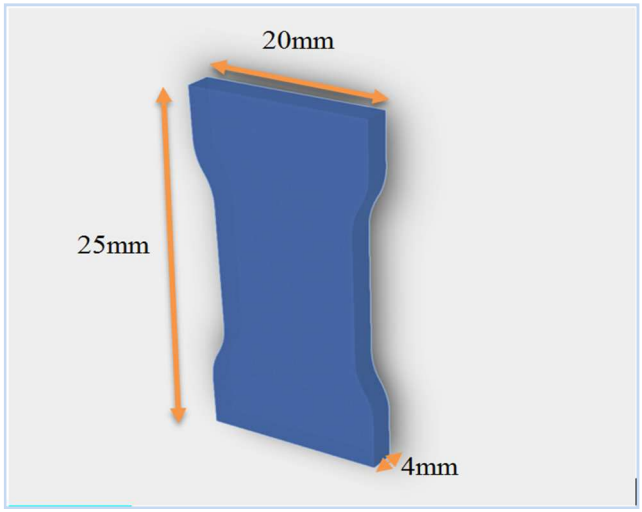

Figure 5 CAD Representation of the Test Part

The test part was designed using Solid Works to be adaptable to both tensile and flexural strength tests. The part dimensions were 2.5cm in length, 2cm width, and 0.4cm in thickness, and is in a dog bone shape configuration, with the ends about 0.3cm wider than the neck. This will ensure that failure will occur in the neck section of the sample. This sample may not have a perfect geometry due to the surfaces not being machined after printing on an FDM machine. Defects occur usually during the print process when the nozzle changes direction due to part geometry, which changes the speed of deposition and the step timing of the stepper motor controlling the filament feed, sometimes leading to defects internally or at the surface. The tests performed using this sample will assume that the build process gives uniform part geometry.

3.1.2 Test Part Print Parameters

Once the part design has been created, the slicing software Slic3r is used to determine the part build parameters. The CAD model is placed on the plater section of the software and is oriented based on the required print direction. Parameters such as infill, layer thickness, nozzle speed, etc., are as shown below in Table 1.

Sl No.	Print Parameters	Values
1	Layer thickness	0.3-0.4mm
2	No. of Perimeters	3
3	Infill Density	100%
4	Infill Pattern	Rectilinear
5	Nozzle Speed	1mm/s – 25m/s
6	Brim width	2m
7	Filament Diameter	3mm
8	Default Extrusion Width	0.5mm

Table 1 Structure Build Parameters

Shown in Table 2 are the temperature dependent print parameters such as nozzle temperature and cooling fan speed. These values are important when correlating interface strength.

Sl No.	Print Parameters	Parameter Values
1	Extruder Temperature	220 ^{0}C
2	Bed Temperature	110 ^{0}C
3	Cooling Fan Speed	35% always

Table 2 Filament Build Parameters

The direction of print should be carefully noted to determine the build part orientation. When the laser heating process is used, the beam spot needs to be in front of the deposition nozzle so that the pre-deposition surface gets heated before the new filament is deposited. Shown in Figure 6 is a schematic of the build process. The current experimental design supports having the spot in front of the nozzle only in the positive X direction. So the part being built is oriented in such a way that there is a pre-heated side, where the pre-deposition surface is heated prior to filament deposition, and the post heated side, where the deposited filament is heated instead of the pre-deposition surface. Strength testing, which will be discussed later will factor this into the testing phase.

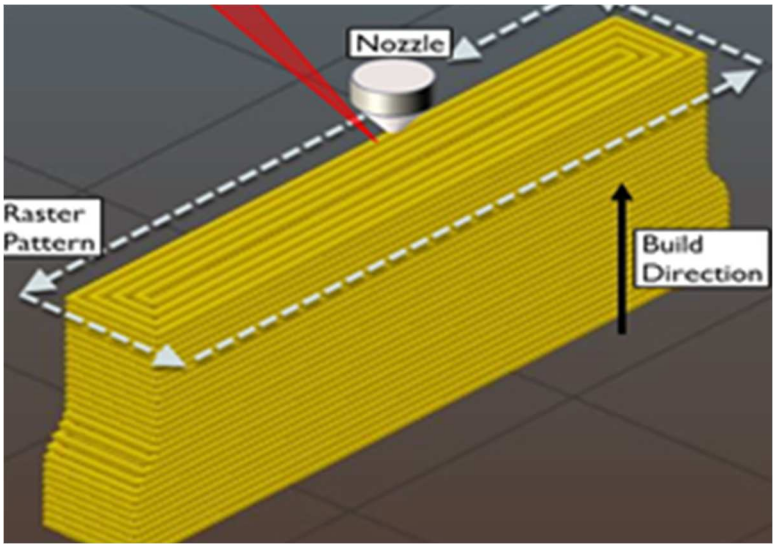

Figure 6 Schematic of the Direction of Nozzle Travel in Relation to the Laser Beam

3.1.3 Design of Laser Optics

The laser optics play a major role in directing the beam from the beam generator to the pre-deposition surface for pre-deposition heating. The laser beam generator is an 802nm solid-state laser with a power rating of 2W. This is a class 4 laser and is handled with care and precautions. A Glan polarizer is used to vary the intensity of laser light by selectively absorbing radiation depending on the user specified rotation angle.

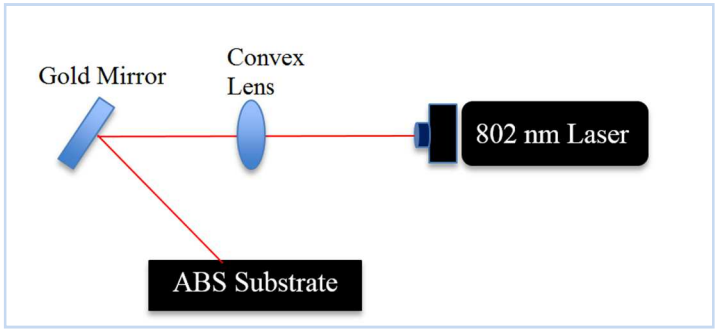

Figure 7 Laser Beam Generator and Optics Setup

The laser beam, after polarization is a divergent beam. This means the intensity distribution of the beam on the pre-deposition surface will not be very precise to carry out localized heating. To converge the beam into a small spot, a glass achromatic convex lens of 100mm focal length and 1" diameter was used. This lens was selected carefully to make sure the wattage of the laser beam generator did not damage it. To direct this converged beam onto the pre-deposition surface, a gold mirror of high precision was used. Since the laser and its associated optics are in a straight line, the angle of the mirror was changed only to move the mirror in the +X or –X direction (direction of nozzle travel). Shown in Figure 7 is the setup of the approach.

3.1.4 Design of Fixtures

The instruments mentioned above need to be positioned and integrated onto the 3D printer without affecting the intrinsic parameters of the FDM process. The 3D printer being used in this research is a Lulzbot mini desktop printer, where the deposition head can move in the X and Z axes, while the deposition bed moves in the Y axis. To decrease uncertainty and errors due to the nature of optics, the fixtures were designed to integrate the Laser beam generator, the lens and the mirror in a way that the Y and Z axes movements can be restricted. As mentioned earlier, the beam spot needs to be in front of the nozzle, which in this case is the +X axis. So it makes sense that the optics has a degree of freedom in the X-axis to accurately position the spot. Shown in Figure 8 and Figure 9 are the fixtures used to support the equipment.

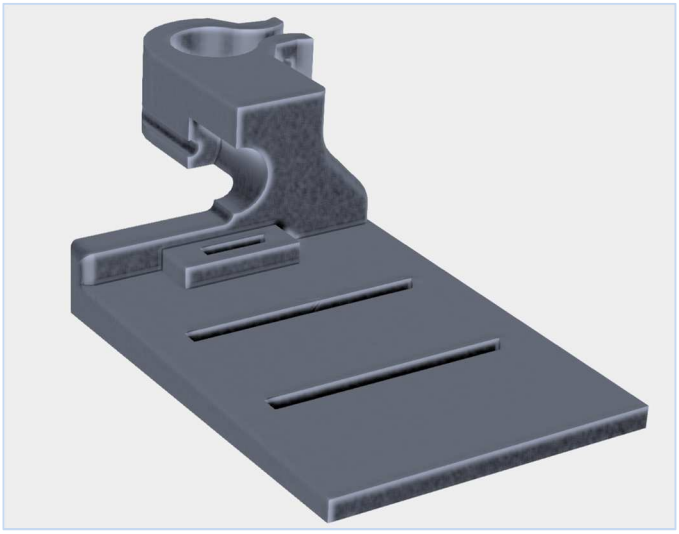

Figure 8 Fixture Design for the Laser Beam Generator

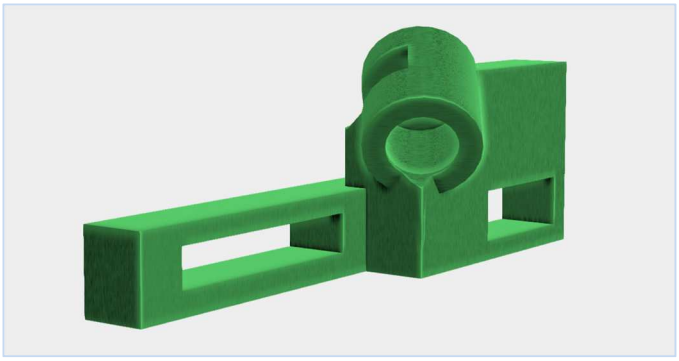

Figure 9 Fixture Design for the Mirror and Lens System

3.2 Temperature Analysis of the Process

The literature review dealt in depth about the effect of interface temperature being a major parameter in determining the strength of the interface, but actual interface temperature data hasn't been collected and analyzed before! Without a correlation between temperature at the interface and the interface strength, the conclusions can be open ended about what is causing the difference in strength. This thesis looks in detail about the temperatures involved in the optical heating approach of the process explained above.

3.2.2 Interface Temperature Profile

With interface temperature being at the helm of the discussion, it is natural to place a great emphasis and effort into obtaining this result. The term interface is the plane between the pre-deposition surface and the deposited material filament. To obtain the temperature values at this junction requires a measurement device, that doesn't hinder or change the deposition process in any way, to avoid errors. To this end, a K type thermocouple was sourced and embedded into the pre-deposition surface using a

molding process, where the surface of the pre-deposition surface was heated above glass transition to properly embed the device. Figure 10 represents a schematic the equipment used for this process. Temperature must be recorded constantly and accurately without a break in time step. The thermocouple was hooked up with a thermocouple breakout board, which converts analog voltage signals into digital. This setup was interfaced with an Arduino Uno, which was calibrated to a data recording time step value of 10 milliseconds. Figure 11 shows the schematic of the experiment.

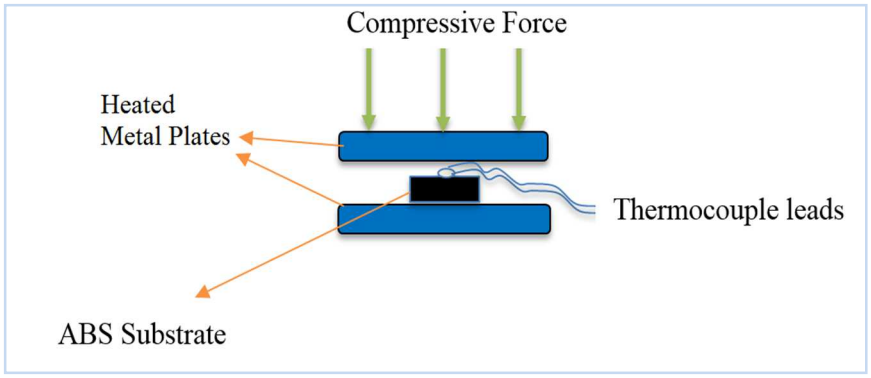

Figure 10 Schematic of Polymer Molding Process

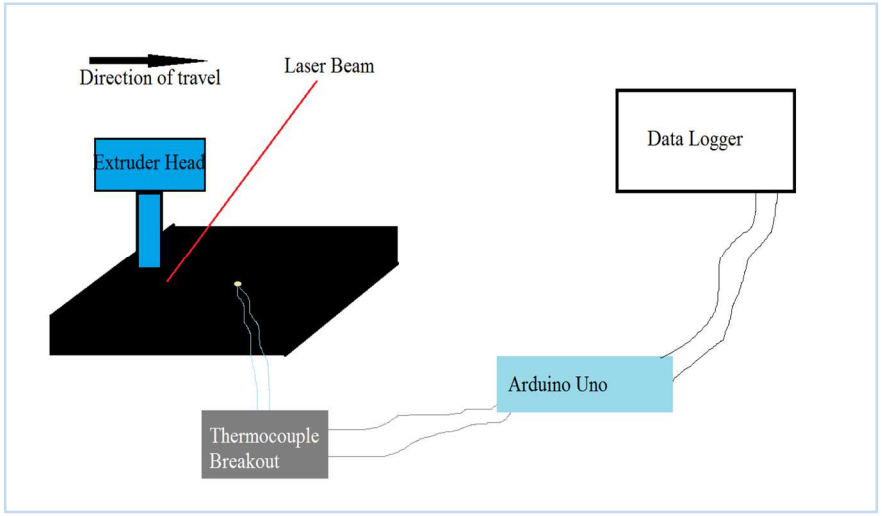

Figure 11 Schematic of Experimental Setup

The experimentation was a direct representation of the process, where the pre-deposition surface, embedded with the thermocouple junction, was scanned by the laser and followed immediately by material filament deposition. What would be observed is an initial spike in temperature, which would signify laser pre-heating of the pre-deposition surface, followed by another temperature reading, which is the true temperature of the interface itself. Based on different conditions like nozzle speed and laser power, the pre-heat temperature might be higher or lower in value when compared to the interface temperature. After obtaining more data, further analysis will be required to understand how surface pre-heating would affect interface temperature, and its correlation to the overall strength of the part.

3.3 Interlayer Strength Characterization

It has been established that interface temperature is a key to improving strength along the interface, and in effect, reduce the anisotropy effect. The true interface temperatures have also been recorded and have to be correlated to the strength data that will be obtained with these sets of experiments.

3.3.1 Effect of Varying Nozzle Speed

Energy Density (ED) is inversely proportional to the nozzle speed, which means that with an increase in speed, the ED on the pre-deposition surface will decrease. This implies that the interface temperature would go down, causing the interlayer strength to decline. To test this theory, a set of experiments was designed where test parts were built as control samples and laser pre-heated samples. The laser power was maintained at a

constant 100% intensity and the nozzle speeds were varied from 2mm/s to 10mm/s. Flexural strength tests were done on both sets of samples, with the pre-heated side facing the tensile loading effect. Shown in Table 3 are the experimental parameters.

Sl No.	Experimental Parameters	Parameter Values
	Control Sample	
1	Print Speed	2mm/s – 10mm/s
2	Laser Power	0 W
	Test Sample	
1	Print Speed	2mm/s – 10mm/s
	Laser Power	0.2 W

Table 3 Part Build Parameters for Nozzle Speed Variation

3.3.2 Effect of Varying Laser Power

A similar set of experiments will be carried out to understand the effect of laser power on the pre-deposition surface. Laser power is directly proportional to ED, and might result in an increase in interface temperature, leading to higher part strength. The experimental parameters are as below in Table 4:

Sl No.	Experimental Parameters	Parameter Values
	Control Sample	
1	Print Speed	5mm/s
2	Laser Power	0 W
	Test Sample	
1	Print Speed	5mm/s
2	Laser Power	0W – 0.2W

Table 4 Part Build Parameters for Laser Power Variation

3.3.3 Interlayer Failure Behavior

By performing flexural strength tests on control and pre-heated samples using 3-point bending test apparatus, it was observed that the control sample failed at a relatively lower flexural strength under loading. Also, there was a clean break observed at the interface when control samples underwent the flexural load test, while the test sample with laser pre-heating had a different failure behavior. Shown in Figure 12 are the images of the surface of the control sample and the laser pre-heated sample, after failure.

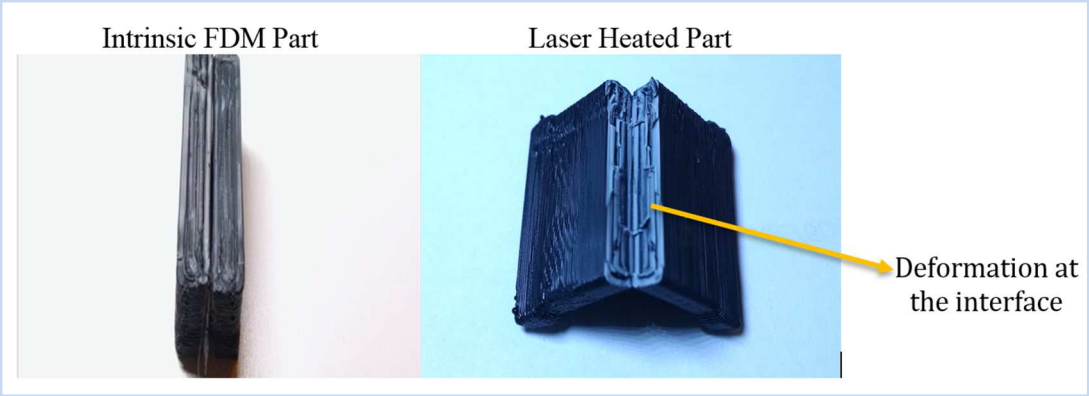

Figure 12 Interlayer Surface Deformation Imaging

This observation required more analysis, with better data to confirm the type of failure involved. Parts were printed with parameters mentioned in Table 5.

Sl No.	Experimental Parameters	Parameter Values
	Control Sample	
1	Print Speed	5mm/s – 25mm/s
2	Laser Power	0W
	Test Sample	
1	Print Speed	5mm/s – 25mm/s
2	Laser Power	0W – 0.2W

Table 5 Experimental Parameters for Part Failure Behavior

These parts were subjected to flexural testing on an Instron 3300 series of tensile tester, which has the capability of recording loading and deflection data over the course of the experiment. The acquired data will be analyzed in more detail to determine whether the control sample exhibits brittle failure behavior, while the laser pre-heated sample exhibits ductile failure behavior. This would give conclusive evidence of increase in diffusion across the interface for the latter case.

3.4 Interlayer Surface Morphology

Section 3.3.3 looked at the deformation occurring at the interface when parts are subjected to flexural tests. This deformation may be caused due to diffusion of polymer chains across the interface, leading to a stronger bond and a disappearance of the so-called interface. To verify this, highly magnified images of the surface were taken using a Scanning Electron Microscope (SEM). Magnifications of 500um and 10um would present a good data set to understand the surface morphology and conclude the degree to which polymer chain diffusion has occurred.

3.5 Road Geometry Analysis

This phase of the study is important to understand the macroscopic effects of laser heating on the pre-deposition surface. Instantaneous optical heating might produce a change in the pre-deposition surface geometry making it a better contact surface for subsequent filament deposition. This may reduce defects formed between two layers, thereby reducing the incidence of stress concentrators. To study this in more

detail, the interlayer surfaces need to be imaged. To obtain the right surface to work with, the part has to be broken clean at the center perpendicular to the build direction. The samples cannot have sheared surfaces, which would produce inaccurate conclusions. To achieve a clean interface, nitrogen freeze fracturing was looked into as an option.

Samples were immersed in a jar of liquid nitrogen till the whole part was frozen. The technic to confirm that the part is fully frozen is to see if nitrogen evaporation has stopped on the sample's surface. Nitrogen has a low vaporization point, and will escape as gasses when they touch a hotter surface. Once the part has been frozen, a notch is created along the direction of fracture, and a load is applied to one side while holding the other in place. This way, a clean fracture would occur to reveal the interlayer surface geometry, which can be imaged under a microscope.

3.6 Laser Ablation Profile Analysis

When laser scanning is performed across an ABS pre-deposition surface, an increase in temperature is expected. At speeds, such as 1mm/s – 5mm/s, and laser intensities like 0.2W, the energy density on the pre-deposition surface is large. Material evaporation has been observed on a large scale. This may influence part strength due to creation of defects, and needs to be addressed.

Due to the Gaussian nature of the beam, intensity distribution is uneven within the beam spot. But increasing the beam spot size using optical means can extend this distribution. The relative position of the converging lens determines the position

of the focal spot on the pre-deposition surface. If the focal spot is on the surface, maximum intensity is at play within a very small area. But if the focal spot is moved away from the pre-deposition surface, for the same laser power, the ED decreases. This concept is illustrated in Figure 13.

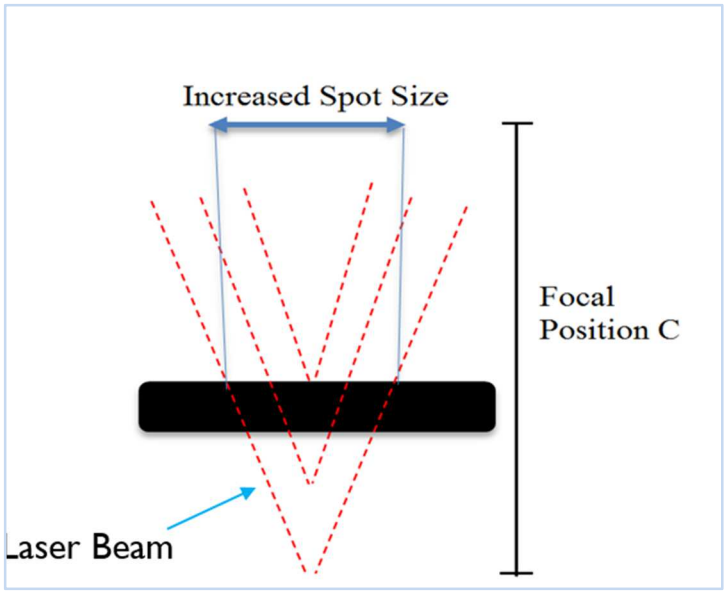

Figure 13 Schematic for Comparing the Effects of Changing Focal Positions

This may cause a reduction in material evaporation and alter the ablation profile to a very shallow form. Optical Profilometry was used to image the laser-ablated surfaces, and experiments were designed to scan a surface with varying nozzle speeds and focal positions. Test conditions have been detailed in Table 6.

Sl No.	Experimental Parameter	Range of values
1	Print speed	5mm/s – 20mm/s
2	Laser Power	0.2W
3	Focal Positions	
	i.	8mm above pre-deposition surface
	ii.	5mm below pre-deposition surface
	iii.	19mm below pre-deposition surface

Table 6 Experimental Parameters for Laser Ablation Profile Analysis

3.7 COMSOL Model Verification

Experiments give accurate real world data that represents the process with all the controllable and uncontrollable factors involved. There are computational models that can be used to predict the interface temperature in the intrinsic FDM process. Since the laser pre-deposition heating approach involves the use of an external parameter, a computational model is required to verify the results we obtain from experiments conducted.

COMSOL is a finite element based software package that can analyze, solve and simulate experimental conditions. It can accept multiple physical conditions and can provide outputs at required probe locations based on user-defined inputs. COMSOL models work based on governing equations and boundary conditions that represent the different physical conditions the model should be simulated within.

Shown below is the governing equation for time dependent heat transfer through a solid.

$$\rho\, Cp \left(\frac{dT}{dt}\right) + \rho\, Cp\, u\, \Delta T = \nabla\,(\mathrm{K}\,.\nabla \mathrm{T}) + \mathrm{Qin} - \mathrm{Qout}$$

Where,

ρ – density of the material

Cp – Specific heat capacity of the material

T – Temperature probe

t – Time probe

u – flow velocity

k – Thermal conductivity

Boundary Conditions:

1) Initial Temperature of pre-deposition surface = 293K

2) Initial Filament Temperature = 503K

3) Q_{out} = Heat lost due to convection

$= h\, A\, (Ts - T\infty)$

4) Q_{in} = Heat input from the laser moving at a constant speed

Table 7 shows the parameters used for generating results in the COMSOL model.

Process Parameters	**Data**
Pre-deposition Surface (PDS) Reflectance	0.2
PDS Absorption Coefficient	200 cm^{-1}
PDS Heat Capacity	1053 J/Kg.K
PDS Thermal Conductivity	0.35W/mK
Laser Scan Speed	5mm/s
Optical Power Input	0.2W
PDS Convective Heat Loss Coeff.	300W/m^2K

Table 7 COMSOL Model Parameters

3.8 COMSOL Parameter Values from Experimentation

The material being used in our experiments is ABS with Carbon Black particles mixed in a 0.03% weight ratio. Literature study did not yield parametric values like heat capacity, thermal conductivity, absorption coefficient, and optical power for the material under study. So these values were calculated using experimental technics in the lab ecosystem.

3.8.1 Heat Capacity Measurement

A sample of carbon black doped ABS was cut and shaped into a cylinder measuring 4mm in diameter and 2mm in thickness. This sample was placed into an aluminum container and placed within a Texas Instrument's QA 2900 DSC measurement system. It is first measured with an empty reference pan and then measured against a sapphire crystal sample. The value obtained has been shown in the table.

3.8.2 Thermal Conductivity Measurement

A sample of carbon black doped ABS was molded and shaped into a cylinder measuring 1inch in diameter and 1.5mm in thickness. A thermal conductivity measurement system built in house was used to conduct measurements. The reported value has been mentioned in the table above.

3.8.3 Absorption Coefficient Measurement

Absorption coefficient value is the inverse of absorption depth. Absorption depth is the distance within a sample at which the incident energy reduces to 35%. A series of samples were prepared with thicknesses varying between 40 microns to 300 microns. A PerkinElmer Lambda 950S UV/VIS/NIR spectrometer was used to detect the sample, which transmits 35% of the incident radiation. The 50-micron sample showed this property and the inverse of this value gives us the absorption depth shown in Table 7.

3.8.4 Optical Power Measurement

The rated wattage of the laser beam generator was 2W, but due to the optics involved, the wattage received at the pre-deposition surface would be lower. A laser power intensity meter was used to detect the maximum laser power, and the value obtained is shown in Table 7.

4. RESULTS AND DISCUSSIONS

4.1 Time Dependent Interlayer Interface Temperature Analysis

Shown in Figures 14, 15, and 16 are time dependent temperature profile measurements for material deposition with control sample as well as test sample conditions at different deposition speeds. The peaks in the graphs occur when the material deposition takes place right above the junction of the thermocouple. Taking the control sample into consideration, the highest temperature was recorded as 76.5°C for the slowest nozzle speed of 5mmps, while the lowest was at 67.75°C for the nozzle speed of 12mmps. This reduction in interface temperature is due the lack of adequate time for the nozzle to pump in enough heat energy into the material filament being extruded. Also, the time required for direct conduction of heat energy from the nozzle to the filament being deposited has also reduced. This trend can also be seen in the same figures, which have an additional component of Laser-pre-deposition heating. Two temperature spikes appear, the first one representing the laser pre-deposition heating of the pre-deposition surface, T1, followed by the second spike T2, which is when the new road is deposited onto the pre-deposition surface. T1 is lower than T2 due to (i) Output Wattage of the laser on the pre-deposition surface, which is only 0.2W based on a laser power meter measurement, and (ii) The Gaussian profile of the beam, which does not heat the pre-deposition surface uniformly. With an increase in nozzle speed, the T1 peaks are less pronounced. Also, as nozzle speeds increase for particular laser intensities, the T1 peak is not easily discernable, both of which are due to a decrease in Energy Density at the pre-deposition surface.

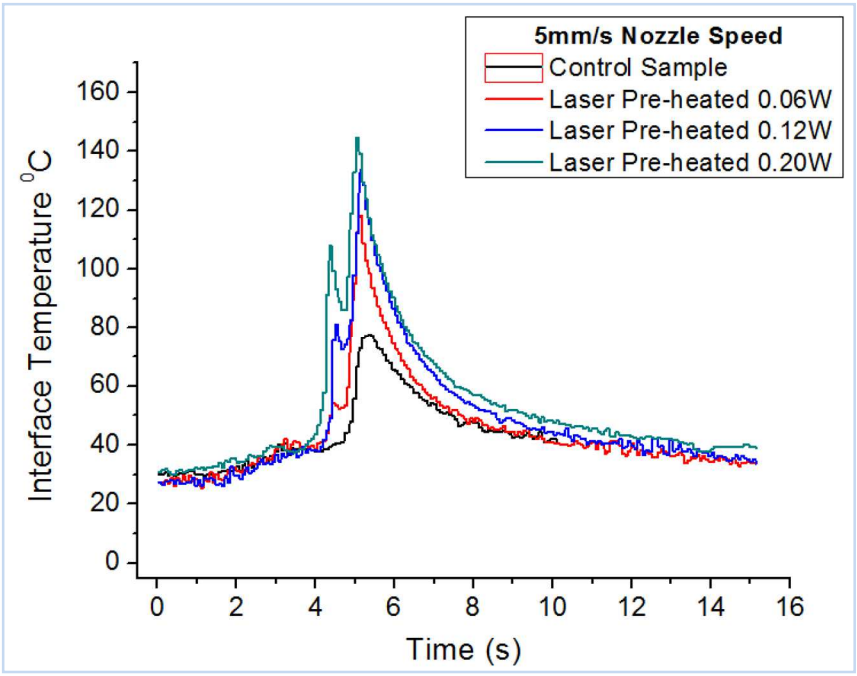

Figure 14 Interface Temperature vs Time Graph for 5mm/s Nozzle Speed

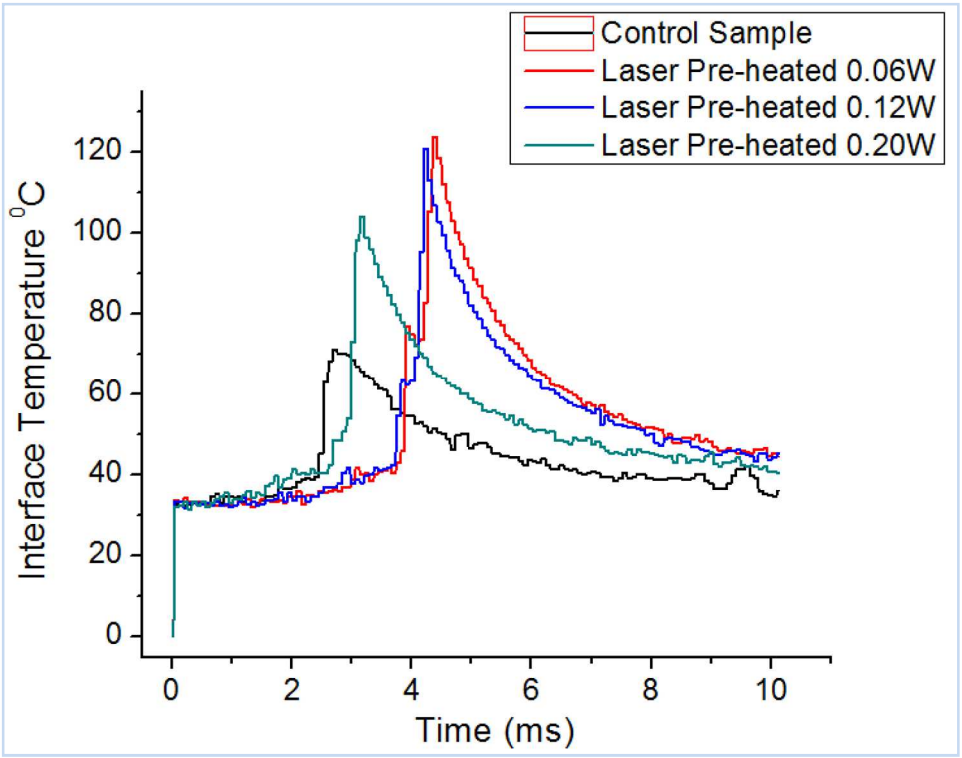

Figure 15 Interface Temperature versus Time Graph for 8mm/s Nozzle Speed

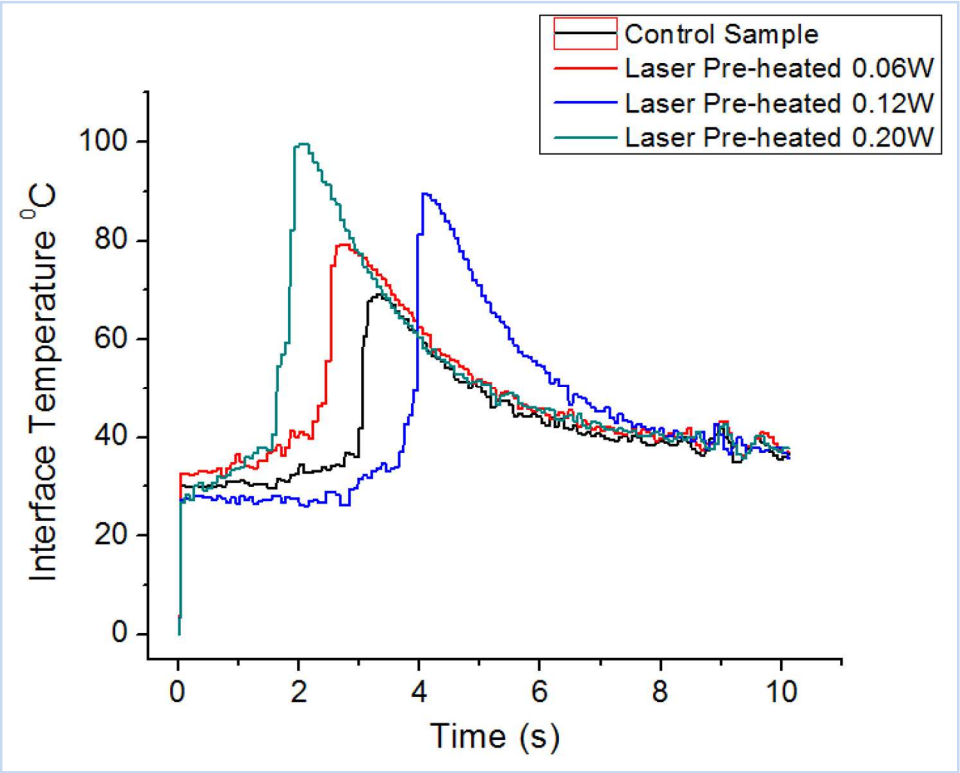

Figure 16 Interface Temperature vs Time Graph for 12mm/s Nozzle Speed

Shown in Figure 17 is a plot between maximum interface temperature and the laser power for three different nozzle speeds. This graph gives us valuable information in terms of the behavior of the interface temperature when pre-heating of the pre-deposition surface is performed. With an increase in temperature, greater polymer chain diffusion is expected. This will be confirmed in the next section with flexural tests on the interlayer interfaces.

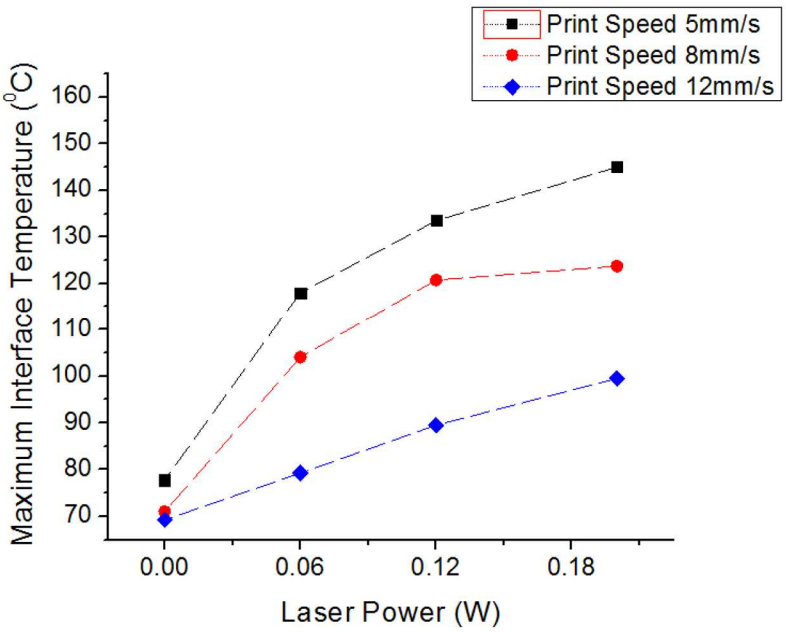

Figure 17 maximum Interface Temperature with Increasing Laser Power

4.2 Flexural Strength Characterization

The results for 3-point bending tests performed on FDM samples, for variation in nozzle speed are shown in Figure 18. The purpose of this test is to understand the difference in strength of samples when the In-process Laser Pre-heating approach is implemented. The control samples built with Intrinsic FDM parameters show lower bending load values when compared to test samples built with Laser Pre-heating. The peak flexural load appears to be increasing with nozzle speed as well for the same laser intensity. There are two effects at play here, namely, thermally assisted polymer chain diffusion, and the temperature and time factor at higher nozzle speeds, both taking place at the layer interface. With an increase in nozzle speed, the cooling time for the roads previously deposited is lower, and this creates a condition where the residual thermal energy fuels more polymer chain diffusion.

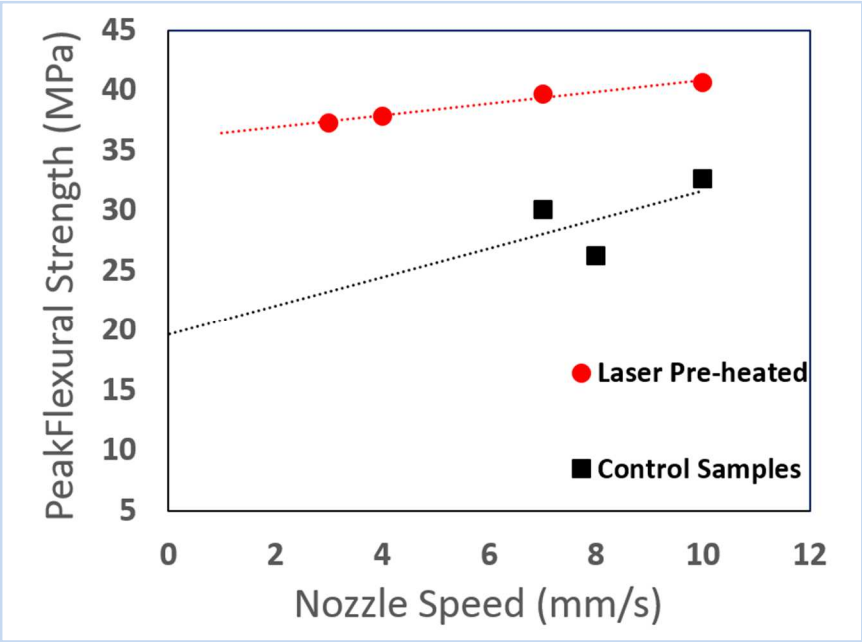

Figure 18 Comparisons of Flexural Strength Test Results for Control Sample and Laser Pre-heated Samples

Shown in Figure 19 are the peak Flexural Strength results of test samples built at the same nozzle speed but with varying laser power intensities. The interaction of the external parameter, i.e. the localized heating by the laser beam, with the pre-deposition surface, has an influence on the strength of the interface itself. As shown below, at a scan speed of 5mm/s, we first see an increase and then a decrease in flexural load with variation in laser power intensity. The initial increase in bending load can be attributed to polymer chain diffusion due to an increase in Energy density. The decrease in bending load for greater laser powers can be due to the fact that material evaporation takes place, which has also been physically observed during experiments. This creates defects on the pre-deposition surface leading to lower part strength. More in depth analysis of these two effects is needed, including the range of speeds and laser intensities for which both effects work in tandem.

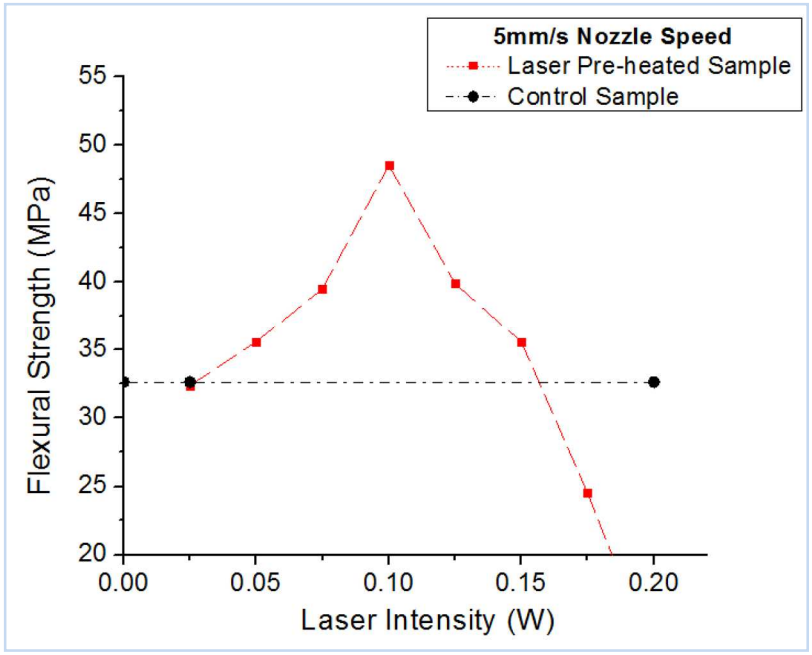

Figure 19 Flexural Strength Data for Samples built at 5mm/s and Multiple laser Powers

Shown in Figure 20 are the bending load versus displacement curves, obtained for samples with laser Pre-deposition heating and intrinsic FDM process. The 2 samples were built with process conditions of 15mm/s nozzle speed and a layer thickness of 400 micron. Results indicate a brittle fracture behavior for the control part, while the test sample with in process laser heating exhibits almost twice the peak bending load and a more ductile fracture behavior. Interlayer interfaces of the control sample are relatively well defined, with lesser polymer chain diffusion, which leads to relatively lesser bending load at the interface. The test sample on the other hand, illustrates greater interlayer strength, highlighted by the larger non-linear fracture curve, which can be attributed to higher polymer chain diffusion fueled by localized laser heating. This increase in strength is statistical evidence that the process works. A closer look at the failure surfaces will be presented later in this discussion.

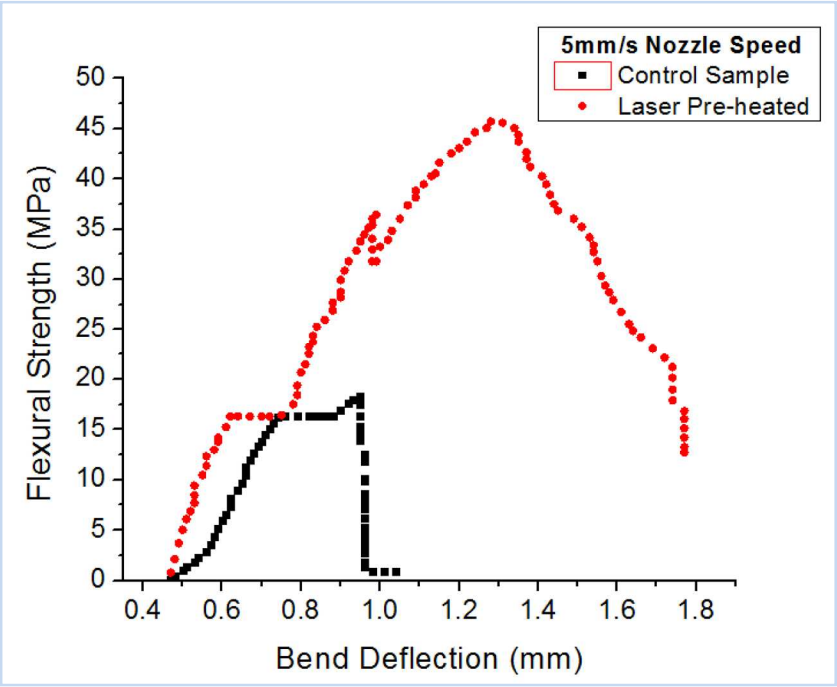

Figure 20 Flexural Strength vs Deflection Graph for Laser Pre-heated and Control Samples

Shown in Figure 21 is the bending load versus deflection graph, which was obtained for samples built with a print speed of 5mmps. As expected, the control sample has the lowest flexural strength and a brittle fracture behavior. With an increase the laser intensity to 75%, the peak flexural strength and ductile fracture behavior reflect the increase, which is due to higher interface strength and polymer chain diffusion. When the laser intensity peaks to 0.2W, there is a decrease in peak flexural strength. At 5mmps and 0.2W Laser intensity, there is material evaporation observed, causing defects to be formed on the pre-deposition surface, which explains the decreased flexural strength data.

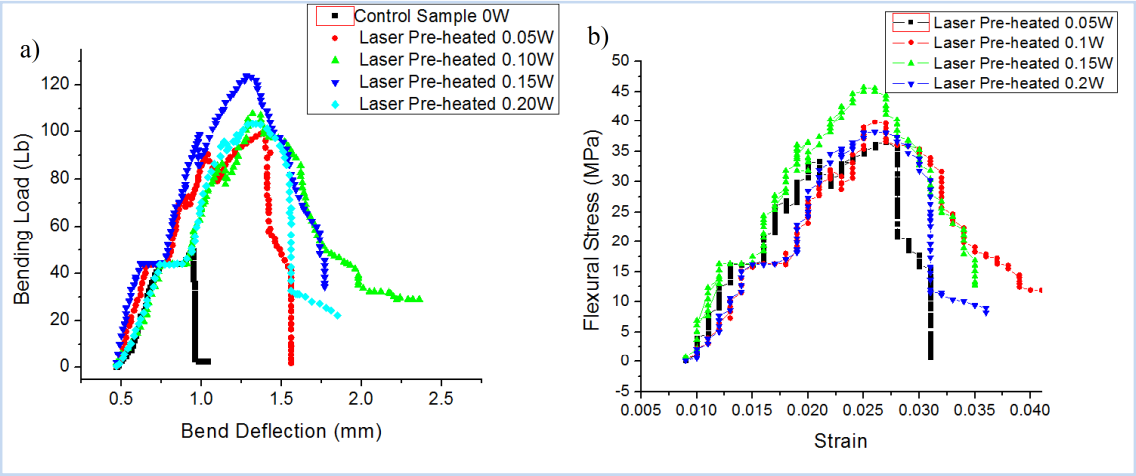

Figure 21 Bending Load and Flexural Stress Graphs for a Nozzle Speed of 5mm/s

Shown in Figures 22, 23 and 24 are the Bending Load vs Deflection data for samples built with print speeds of 10mm/s, 15mm/s and 20mm/s. An observation, which can be made here, is that unlike the graphs for 5mm/s, the plots for these print speeds show a logical trend in peak bending load values, in that they increase with higher Laser intensities. A quick revisit to the concept of Energy Density [ED], which represents the total amount of energy received at the pre-deposition surface when the laser scans across it, and is dependent on the Nozzle speed and laser intensity.

$$Ed = (2P) / (\pi\, r\, V)$$

where,

Ed – Energy Density

P – Incident Laser Power

r – Radius of the Laser Beam

V – Velocity of Laser Beam Travel

With an increase in nozzle speed, the graphs move towards higher flexural strength values. To explain this, there are 4 effects that need to be addressed here:

When the filament material is moving,

1) Reduced Heat conduction into the pre-deposition surface
2) Time dependent cooling of adjacent filaments during deposition

When the filament material is stationary,

3) Heat transfer by conduction at the layer interface
4) Mass Transfer by Diffusion of Polymer chains

During the extrusion process, there are two segments of the extrudate to consider, i.e., the filament right below the nozzle, which is dynamic in behavior, and the filament at a distance from the nozzle, which is relatively stationary. The first segment involves effects (1) and (2), while the latter displays effects (3) and (4) in greater significance when compared to effects (1) and (2). A point to note here is that the effect due to material advection, may not be a valid assumption here, as even at speeds of 25mm/s, the flow is quite laminar. A deeper look into flow patterns and rheology is required to confirm this. We can instead assume that with faster speeds, the adjacent roads will still have some thermal capacity to promote polymer chain diffusion.

Taking any one speed into consideration, with increasing laser intensity, pre-deposition surface temperature increases thereby boosting the effects (3) and (4) leading to formation of stronger bonds at the interface. But with increasing nozzle

speed, there is an increase in peak bending load strength observed in Figures 22, 23 and 24 which is counter-intuitive due to reduced energy density on the pre-deposition surface, both with and without the in-process laser heating. This can be reasoned by looking towards effect (2), which is the remaining thermal energy in adjacent roads prior to deposition, which would play a role in increasing the interface bond strength. Thus, with an increase in speed, it has been observed that flexural strength increases.

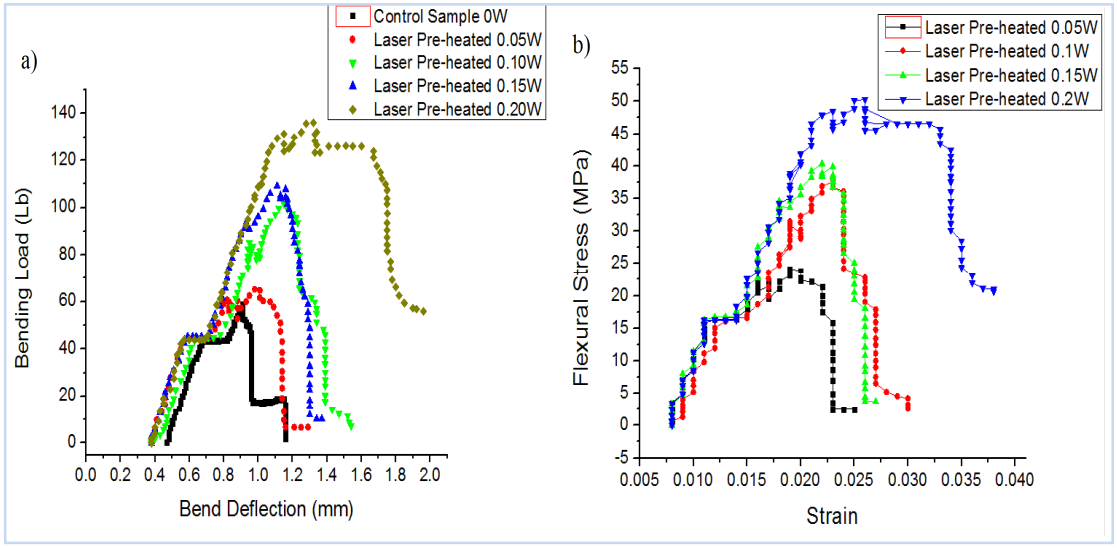

Figure 22 Bending Load and Flexural Stress Graphs for a Nozzle Speed of 10mm/s

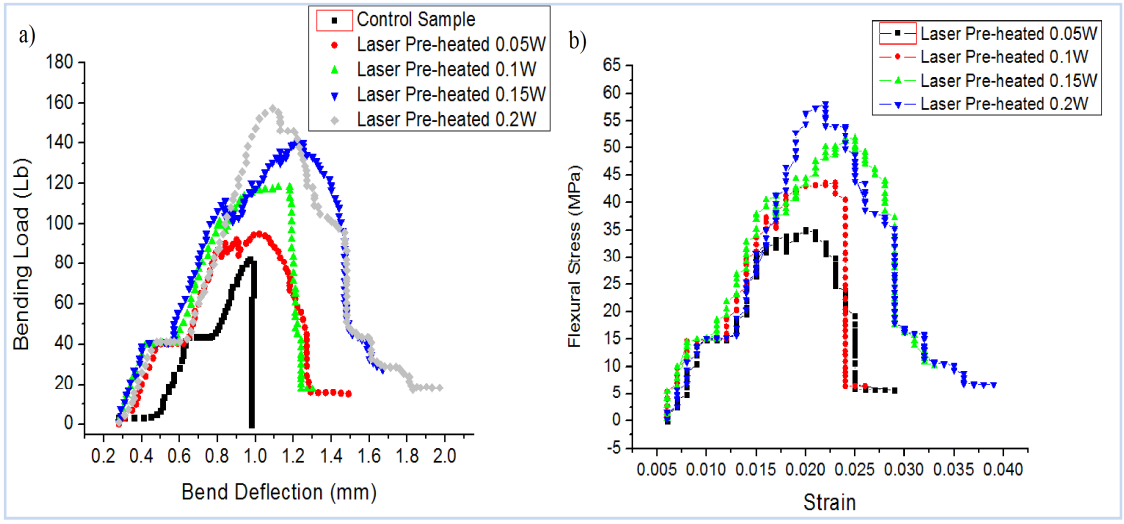

Figure 23 Bending Load and Flexural Stress Graphs for a Nozzle Speed of 15mm/s

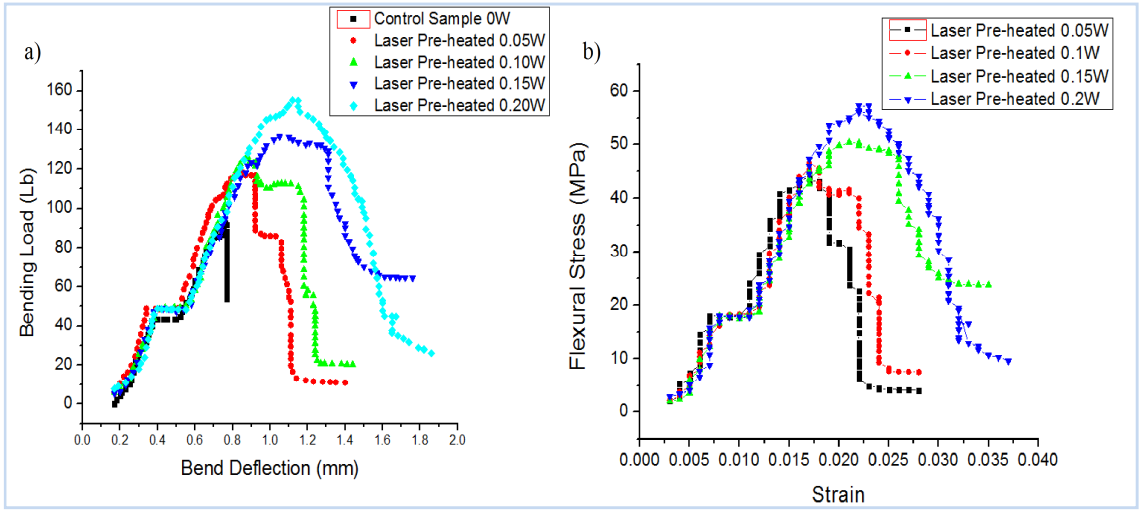

Figure 24 Bending Load and Flexural Stress Graphs for a Nozzle Speed of 20mm/s

Shown in Figure 25 are the peak Flexural Strength values versus Laser intensity graphs for a range of nozzle speeds. A closer look at the graphs for 5mm/s, for laser powers of 0.05W to 0.15W, shows a drastic increase in flexural strength when compared to 10mm/s. This is because the energy density received for 5mm/s is greater than for 10mm/s, which points to the fact that laser pre-heating at the pre-deposition surface has induced higher interface temperatures, leading to greater polymer chain diffusion

between the layers. When the laser power approaches 0.2W, material evaporation is observed for 5mm/s nozzle speed, which causes the decrease in flexural strength, while the flexural strength is higher for 10mm/s nozzle speed. For nozzle speeds of 15mm/s and 20mm/s, we see a rise and a decrease in the slope of the peak loads. The reason behind this is due to the ED received at the pre-deposition surface, which decreases with an increase in speed. The energy density is adequate to induce more diffusion of polymer chains without significant material evaporation, which explains the reduction in slope value of the curves. In an overall sense, a relation between Bending Load and Laser Intensity can be obtained, when there is no material-evaporation taking place, and this can predict the optimum conditions for a part requiring a high bending load for failure!

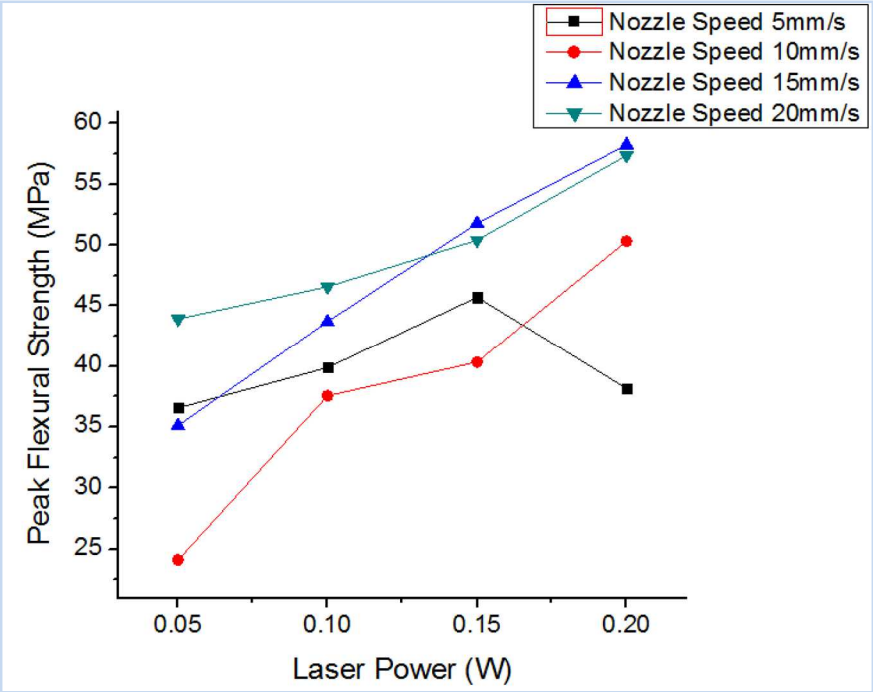

Figure 25 Peak Flexural Strength vs Laser power for Different Nozzle Speeds

Shown in Figure 26 is the direction depiction of the effect of increase in interface temperature on the interlayer flexural strength. Brittle fracture behavior and a lower peak flexural stress is detected for the control sample while the laser-heated sample displays higher peak flexural strength and a ductile behavior.

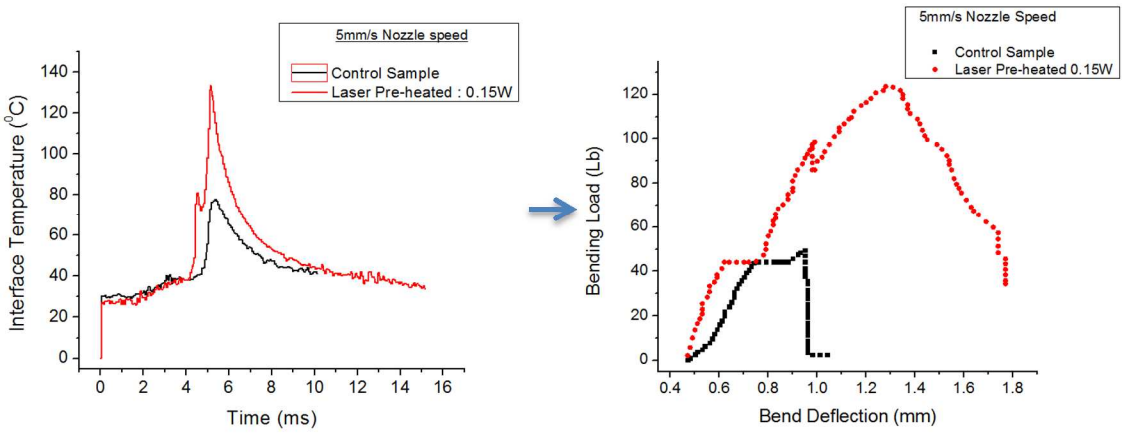

Figure 26 Interface Temperature and Interlayer Strength Correlation

4.3 Interlayer Surface Morphology

Shown in Figure 27 are the Scanning Electron Microscope images of the interface, for both the control sample and a laser pre-heated sample. It is observed that the control sample has a cleaner structure at the interface, with failure occurring in between 2 subsequent layers. The 500micron image shows a smooth surface with most of the filament structure intact. The 10micron image shows very less deformation on the surface, implying that relatively lower polymer chain diffusion has occurred at this interface for this sample. The lumps on the surface may be representative of the polymer chains bundled together, without crossing the interface. In comparison, the laser pre-heated sample shows failure occurring across multiple layers, which has established that polymer chain diffusion has occurred over a much larger and deeper area! The

500micron image shows the filament structure in a relatively more deformed state and the 10micron image shows a very rough surface at the interface. This may be due to the fact that polymer chains have crossed the interface, and the fracture occurred through the path of least resistance. Based on the results presented earlier, a combination of higher speeds and greater laser intensity would create an interface with much larger polymer chain diffusion.

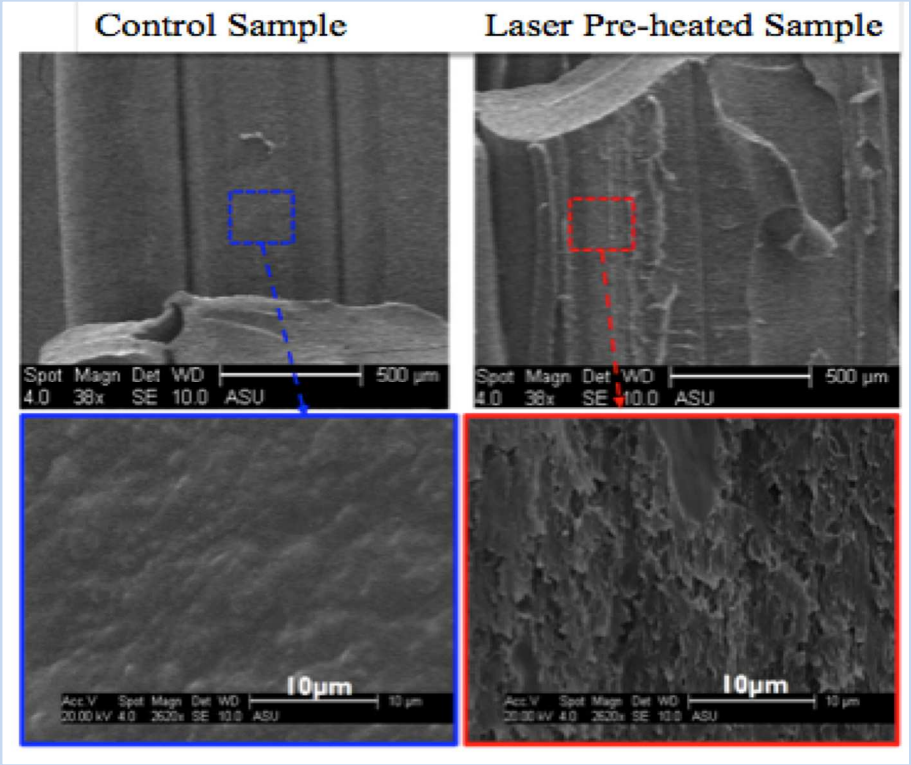

Figure 27 SEM Images of the Fracture Interface

4.4 Road Geometry Analysis

The aim of this process is to achieve greater isotropy in flexural strength of the part by pre-heating the pre-deposition surface to increase polymer chain diffusion. While the flexural strength data has given evidence of this, there has been another observation to note, i.e., the geometry of the interface. Shown in Figure 28 is the image of the cross section of samples, with multiple layers, where a pre-determined combination of Natural ABS and Black ABS were used to get a clearer image of the interface geometry. The image on the left represents a control sample, built with intrinsic FDM process parameters while the image on the right represents a test sample with in-process laser heating of the pre-deposition surface [Black ABS]. As seen in the figure, the roads have oval shaped geometric boundaries, which introduces defects within and in-between layers. This decreases the surface area of contact between roads thereby reducing the interface area for polymer chain diffusion. With laser pre-deposition heating on the pre-deposition surface, the defects/voids are reduced significantly, to the tune of 37%, and an approximate 9.15% increase in pre-deposition surface deposition length is observed. The decrease in void area shows that the laser heating process has changed the road geometry by reheating the surface, thereby making the pre-deposition surface smoother for the subsequent filament deposition to take place. Also, the interface contact area has increased by 28% for these process conditions. This gives polymer chain diffusion more contact surfaces to occur in, thereby increasing the interface strength. These results show that implementing laser pre-heating at the pre-deposition surface leads to better deposition and interaction surface.

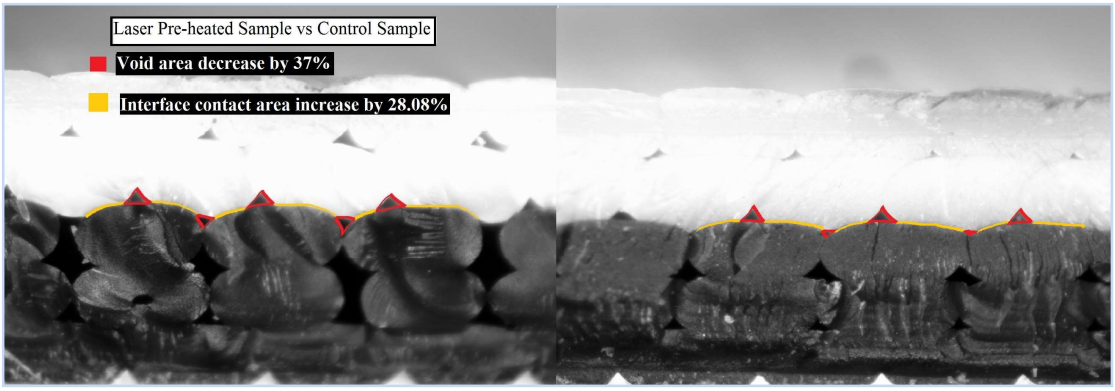

Figure 28 Road Geometry Analyses

4.5 Laser Ablation Profile Analysis

The results shown above talk about the Bending load between the layers, and the factors that influence it, i.e., polymer chain diffusion and layer interface temperature. Ideally, pre-heating the pre-deposition surface using the optical method to a large value without material loss would drive up the interface temperature, leading to a very homogenous interface geometry, where the interface itself may disappear, thereby, assuming material properties. Practically, in the present optical setup, the Gaussian profile of the beam causes material evaporation, leading to a trench type profile to be formed on the pre-deposition surface. There are 3 factors at play here, i.e. 1) focal spot position of the lens and 2) speed of travel by the nozzle, and 3) laser power, which determine the Energy Density. Of these, (1) and (2) are variables which are controlled by the user.

Figure 29 represents an optical profilo-metry image of the pre-deposition surface when ablated with the 802nm laser at a speed of 5mm/s, at 3 different focal lengths, and at the highest laser power of 0.2W. The focal spot is at 3 positions, i.e. i) 8mm above the pre-deposition surface, ii) 5mm below the pre-deposition surface and iii) 19mm below the pre-deposition surface. Focal position (ii) exhibits the maximum depth profile while position (iii) reveals a shallower profile in every case of nozzle speed. This is because the focus is closest to the pre-deposition surface, which is the situation for case (ii), and this cause higher energy density due to a smaller spot size on the surface.

Observe the material build up on either side of the trenches, which is due to material warping and melt reflow due to the heating intensity and spot size of the laser beam on the pre-deposition surface. Focal position (ii) shows that the pre-deposition surface is exposed to a far greater ED when compared to (iii), leading to larger material evaporation and displacement. Also, as the nozzle speed increases, there is an observable decrease in the depth of ablation, which is again due to a reduced energy density on the pre-deposition surface. This is shown in Figure 30. For all laser scan speeds, focal position (iii) offers the smallest material evaporation profile, which will help reduce the incidence of defects in the build volume.

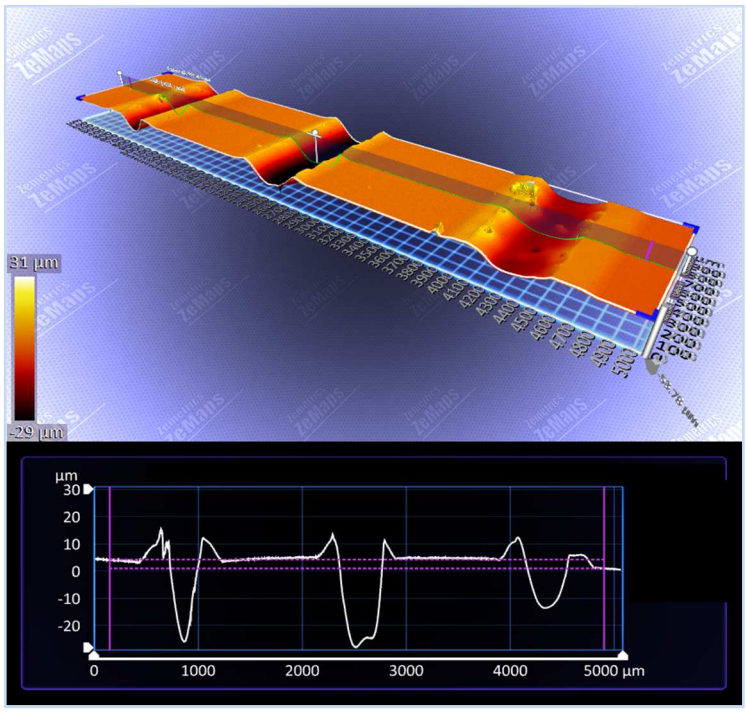

Figure 29 Laser Ablation Profile Obtained from the Optical Profilo-Meter

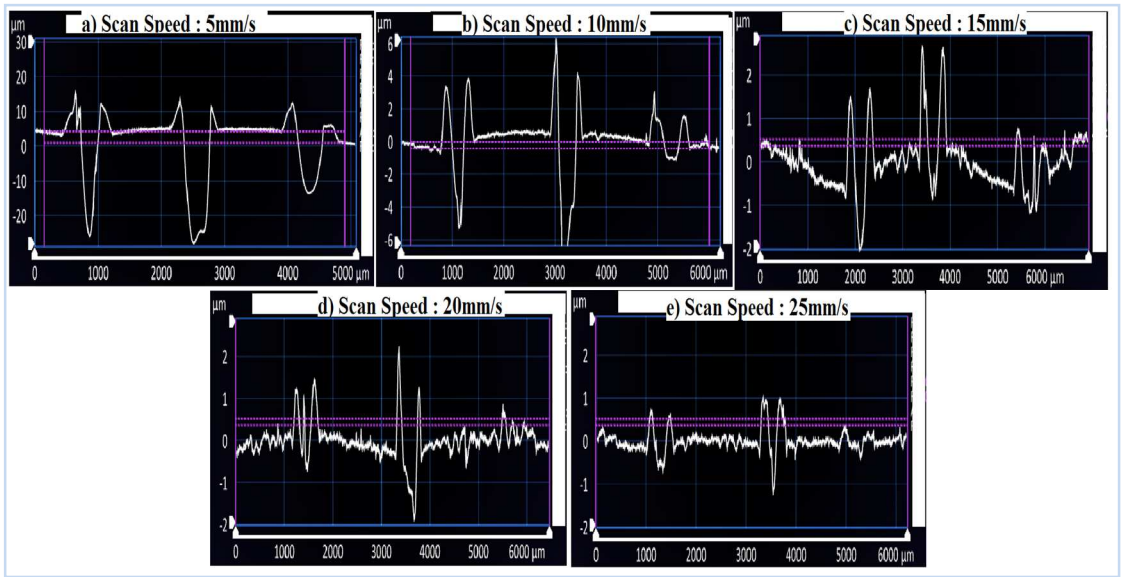

Figure 30 Ablation Depth Measurements for Different Scan Speeds

Shown in Figure 31a is the volumetric optical profilometry image of a 5mmps focal position (i) laser scan profile. The volume displaced in a particular area of the profile has been estimated as 0.0047mm^3 and the volume build up outside the trench is 0.0014mm^3. The evaporation of material in this case is the difference of the values above, and is quantified as 0.0033mm^3, which is quite sizable! After imaging laser scans of 5mmps and 10mmps, at different focal positions (a, b and c), a graph between Evaporation volume and scan speed has been plotted, which is shown in Figure 31b. The trend line shows us an approximate direction in which the process needs to be tuned to minimize material evaporation, which is by increasing the scan speed or the focal position. More detailed studies need to be done on the temperature effects on the pre-deposition surface when these process conditions are employed.

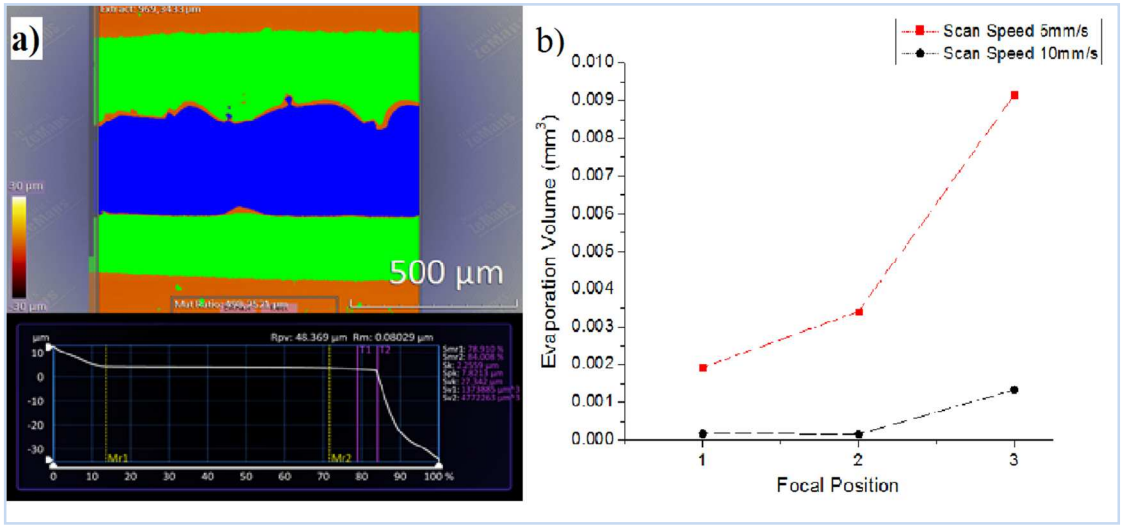

Figure 31 Volumetric Material Evaporation Analyses

4.6 COMSOL Model Verification of Experimental Data

Based on the process conditions, the result from the COMSOL model has been displayed in Figure 32.

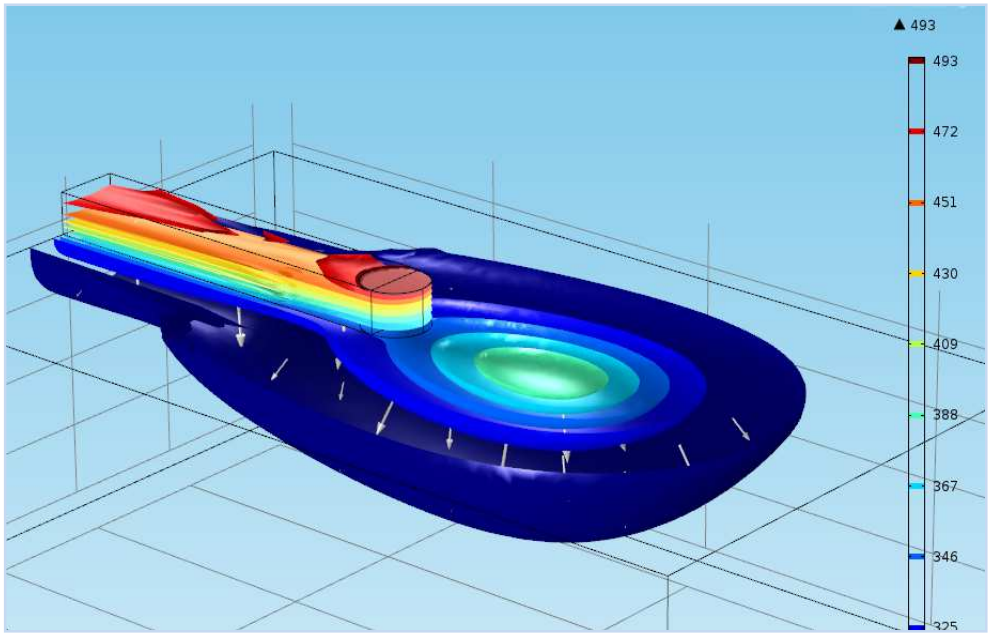

Figure 32 Results of the COMSOL Model Setup

The pre-deposition heating temperature results obtained from the COMSOL model is very close to the values obtained experimentally. Shown above are temperatures for a nozzle speed of 5mm/s and a laser power of 0.2W. The maximum temperature is at the filament deposition surface, which is 220 degree Celsius. The temperature of the pre-deposition surface where the laser beam is incident is at 388K or 115 ^{0}C, and is very close to the results obtained with the thermocouple, which was 113 ^{0}C. To obtain the interface temperature, more study and work is required to be done on the COMSOL model.

CONCLUSION

The goal of the thesis was to reduce FDM part anisotropy by optical heating of the pre-deposition surface, to locally increase the interface temperature, and thermally induce polymer chain diffusion across the interface. The process was implemented onto a desktop 3D printer and the optics was tuned to produce the desired effects. Experiments were designed to look at the pre-deposition surface and interface temperature profiles, which were obtained for various speeds and laser powers. Energy Density of the laser beam influenced the interface temperatures, which tended towards higher values with an increase in ED. Flexural strength tests were performed on samples under different process conditions to understand the effects of the intrinsic and the external parameters on the polymer chain diffusion process. By pre-deposition laser heating, interface strength increased by around 50% over control samples. An increase in nozzle speed saw a corresponding increase in flexural strength required to break the bonds at the interface, which may have been due to residual temperature effects. To understand the failure behavior, FDM built parts were loaded, and the deflection data was recorded and analyzed. Control samples exhibited a brittle fracture behavior while laser heated samples showed a ductile fracture behavior. Morphology of the fracture surfaces was analyzed to confirm the above. One other factor influencing part strength was material evaporation. Focal positions of the laser spot were changed to bring about a corresponding change in energy density, which controlled material evaporation. The ablation profile was captured using an optical profilo-meter, and analyzed to determine conditions to minimize material loss at the pre-deposition surface.

A lot of work was performed to understand the effects of pre-deposition laser heating process on interlayer strength. This thesis has provided a base for the process to grow more sophisticated, analytical and predictive. With an array of parametric results in hand, future studies can be planned to quantify more aspects of the process and improve the isotropy of FDM built parts.

FUTURE WORK AND RECOMMENDATIONS

The results presented here have shown an increase in FDM part isotropy, when the optical pre-deposition heating system was implemented. Future work would involve getting a deeper understanding of the process parameters and their effects, as well as improve the design of the system.

- One major issue affecting both the temperature being recorded and the part strength was material evaporation, which varied between lower and higher energy densities. A combination lens system can be proposed, where a divergent lens is placed at a pre-determined distance from the convex lens to produce a collimated beam with a rectangular cross section. This way, the intensity distribution within the beam spot will be uniform, and the material evaporation profile can be manipulated easily.
- For the interface temperature measurements with the thermocouple, the laser beam is briefly incident on the junction instead of the pre-deposition surface. Absorption property of the thermocouple is lower than the ABS+CB surface, and this needs to be factored into future temperature measurements and analyses.
- The power produced by the 802nm laser at the pre-deposition surface was measured to be only 0.2W, which is much lower than the actual 2W rating. The parameters influencing this drop in power should be studied in more detail to determine the setup conditions to obtain higher power from the same solid-state laser. This would possibly drive up interface temperatures to higher values, which would effectively increase the interface temperature.

- Rheology of the ABS polymer material needs to be looked into, to understand how temperature affects the flow of polymer chains across the interface. Flow parameters would affect diffusion of polymer chains and can be manipulated to increase this diffusion.
- SEM images of the ablated road surfaces can be performed to understand the thermal expansion and melt reflow of material when a sudden increase in temperature occurs. A set of experiments can work towards reducing the changes in the surface geometry to reduce the incidence of defects.
- At higher nozzle speeds, it is observed that parts gain a relatively higher strength between 2 layers. This may be due to the print conditions where the deposited roads have residual heat, which would provide a base for more polymer chain diffusion across the interface. A study has to be performed on this effect.
- Freeze fracturing of samples with liquid nitrogen was performed to look at the interlayer surface geometry without compromising the features within. This process needs to be more controlled to obtain cleaner and defect free surfaces to image.

REFERENCES

1. Agarwala, M., Jamalabad, V., et. al., "Structural quality of parts processed by fused deposition", Rapid Prototyping Journal, Vol. 2 No. 4, pp. 4-19. (1996)

2. Langrana, N., Qiu, D., et. al., "Virtual simulation and video microscopy for fused deposition methods", Material and Design, No. 21, pp.75-82. (2000)

3. Anitha, R., Arunachalam, S., Radhakrishnan, P., (2001), "Critical parameters influencing the quality of prototypes in fused deposition modelling" Journal of Materials Processing Technology. Vol 118, pp. 385-388. (2001)

4. Bose, S., Darsell, J., et. al. (2002), "Pore size and pore volume effects on alumina and TCP ceramic scaffolds", Material Science and Engineering, C 23, pp. 479-486. (2002)

5. Darsell, J., Susmita, B., et. al., "From CT Scan to Ceramic Bone Graft", Journal of American Ceramic Society, Vol. 86 No. 7, pp. 1076-80. (2003)

6. Bellini, A., Shor, L. and Guçeri, S., "New developments in fused deposition modeling of ceramics", Rapid Prototyping Journal, Vol. 11 No.4, pp. 214-220. (2005)

7. Wu, G., Langrana, N.A., Sadanji, R., and Danforth, S., "Solid freeform frabrication of metal components using fused deposition of metals", Materials and Design, Vol. 23, pp.97-105. (2002)

8. Yan, Y., Rendong, W., et. al., "Biomaterial forming research using RP technology", Rapid Prototyping Journal, Vol. 9 No. 3, pp.142-149. (2003)

9. Bellini, A., and Guçeri, S., "Mechanical characterization of parts fabricated using fused deposition modeling", Rapid Prototyping Journal, Vol. 9 No. 4, pp. 252-264. (2003)

10. Rodriguez, J.F., Thomas, J.P. and Renaud, J.E., "Characterizing the microstructure of fused deposition polymer components", CAE and Intelligent Processing of Polymeric Materials, MD-Vol. 79, ASME, NY, pp.299-308. (1997)

11. Rodriguez, J.F., Thomas, J.P. and Renaud, J.E., "Tailoring the mechanical properties of fused-deposition manufactured components", Proc. Rapid Prototyping and Manufacturing '99, Vol. 3, Society of Manufacturing Engineers, Dearborn, MI, pp.629-43. (1999) □

12. Rodriguez, J.F., Thomas, J.P. and Renaud, J.E., "Design of Fused-Deposition ABS Components for Stiffness and Strength", Journal of Mechanical Design, Vol. 125, pp.545-551. (2003) □

13. Yan, Y., Zhang, R., Guodong, H., and Yuan, X., "Research on the bonding of material paths in melted extrusion modeling", Materials and Design, Vol. 21, pp. 93-99. (2000) □

14. Anitha R, Arunachalam S, Radhakrishnan P (2001) Critical parameters influencing the quality of prototypes in fused deposition modelling. J Mater Process Technol 118(1–3):385–388

15. Nancharaiah T, Raju DR, Raju VR (2010) An experimental investigation on surface quality and dimensional accuracy of FDM components. Int J Emerg Technol 1(2):106–111

16. Thrimurthulu K, Pandey PM, Reddy NV (2004) Optimum part deposition orientation in fused deposition modeling. Int J Mach Tools Manuf 44(6):585–594

17. Horvath D, Noorani R, Mendelson M (2007) Improvement of surface roughness on ABS 400 polymer using design of experiments (DOE). Mater Sci Forum 561:2389–2392

18. Wang CC, Lin TW, Hu SS (2007) Optimizing the rapid prototyping process by integrating the Taguchi method with the gray relational analysis. Rapid Prototyp J 13(5):304–315

19. Sood AK, Ohdar R, Mahapatra S (2009) Improving dimensional accuracy of fused deposition modelling processed part using grey Taguchi method. Mater Des 30(10):4243–4252

20. Zhang JW, Peng AH (2012) Process-parameter optimization for fused deposition modeling based on Taguchi method. Adv Mater Res 538:444–447

21. Sahu RK, Mahapatra S, Sood AK (2013) A study on dimensional accuracy of fused deposition modeling (FDM) processed parts using fuzzy logic. J Manuf Sci Prod 13(3):183–197

22. Lee B, Abdullah J, Khan Z (2005) Optimization of rapid prototyping parameters for production of flexible ABS object. J Mater Process Technol 169(1):54–61

23. Laeng J, Khan ZA, Khu SY (2006) Optimizing flexible behavior of bow prototype using Taguchi approach. J Appl Sci 6:622–630

24. Zhang Y, Chou K (2008) A parametric study of part distortions in fused deposition modelling using three-dimensional finite element analysis. Proc Inst Mech Eng Part B 222(8):959–968

25. Nancharaiah T (2011) Optimization of process parameters in FDM process using design of experiments. Int J Emerg Technol 2(1):100–102

26. Kumar GP, Regalla SP (2012) Optimization of support material and build time in fused deposition modeling (FDM). Appl Mech Mater 110:2245–2251

27. Ahn SH, Montero M, Odell D et al (2002) Anisotropic material properties of fused deposition modeling ABS. Rapid Prototyp J 8(4):248–257

28. Ang KC, Leong KF, Chua CK et al (2006) Investigation of the mechanical properties and porosity relationships in fused deposition modelling-fabricated porous structures. Rapid Prototyp J 12(2):100–105

29. Sood AK, Ohdar RK, Mahapatra SS (2010) Parametric appraisal of mechanical property of fused deposition modelling processed parts. Mater Des 31(1):287–295

30. Percoco G, Lavecchia F, Galantucci LM (2012) Compressive properties of FDM rapid prototypes treated with a low cost chemical finishing. Res J Appl Sci Eng Technol 4(19):3838–3842

31. Rayegani F, Onwubolu GC (2014) Fused deposition modelling (FDM) process parameter prediction and optimization using group method for data handling (GMDH) and differential evolution (DE). Int J Adv Manuf Technol 73(1–4):509–519

32. Masood SH, Mau K, Song WQ (2010) Tensile properties of processed FDM polycarbonate material. Mater Sci Forum654:2556–2559

33. Rodriguez, J.F., Thomas, J.P. and Renaud, J.E., "Tailoring the mechanical properties of fused-deposition manufactured components", *Proc. Rapid Prototyping and Manufacturing '99*, Vol. 3, Society of Manufacturing Engineers, Dearborn, MI, pp.629-43. (1999)

34. Yan, Y., Zhang, R., Guodong, H., and Yuan, X., "Research on the bonding of material paths in melted extrusion modeling", *Materials and Design*, Vol. 21, pp. 93-99. (2000)

35. Seth Partain, Fused Deposition Modeling with Localized Pre-Deposition Heating Using Forced Air, Master's Thesis, Montana State University, 2007

36. P. G. De Gennes, " Reptation of a polymer chain in the presense of fixed obstacles," the Journal of Chemical Physics, 572, 1971

37. Wool, R.P., Yuan, B.L. and MacGarel, J., "welding of polymer interfaces," Journal of Polymer Engineering and Acience, V.29, pp. 1340 (1989)

38. [7], p.95